Cancer Nanotechnology

RESEARCH Open Access

Construction of pH-responsive nanocarriers in combination with ferroptosis and chemotherapy for treatment of hepatocellular carcinoma

Huan Yue[1,5†], Luxia Gou[2†], Zhenrong Tang[3†], Yuyang Liu[4], Shengchun Liu[3*] and Hua Tang[1*]

*Correspondence: liushengchun1968@163.com; tanghua86162003@cqmu.edu.cn
†Huan Yue, Luxia Gou, and Zhenrong Tang have contributed equally to this work
[1] Key Laboratory of Molecular Biology for Infectious Diseases (Ministry of Education), Institute for Viral Hepatitis, Department of Infectious Diseases, The Second Affiliated Hospital, Chongqing Medical University, 1 Yi Xue Yuan Road, Chongqing 400016, China[3] Department of Endocrine and Breast Surgery, The First Affiliated Hospital of Chongqing Medical University, Chongqing, China
Full list of author information is available at the end of the article

Abstract

Background: Chemotherapy is widely used to treat hepatocellular carcinoma (HCC). Although sorafenib (SO) is the only chemotherapy drug approved by FDA for treatment of HCC, it is associated with several disadvantages including low water solubility, low bioavailability, lack of targeting and easily causes systemic toxicity. In recent years, nanocarriers have shown promise in drug delivery to effectively solve these problems. Herein, we used SO-loaded nanocarriers to overcome the defects of chemotherapy during treatment of HCC. Specifically, we encapsulated pH-sensitive hollow mesoporous Prussian blue nanoparticles (HMPB) with SO (an inhibitor of multi-kinase and accelerant of ferroptosis) to act as carriers and facilitate drug release. We also coated its surface with a layer of pH-responsive chitosan (CS) to block the drug and increase biocompatibility. Finally, we successfully constructed HP/SO/CS nanocomposites for targeted delivery of chemotherapeutic drugs, with the aim of initiating chemotherapy and ferroptosis for dual treatment of tumors. In vitro and in vivo experiments were performed for evaluation of the nanocomposites' anti-tumor efficacy by using liver cancer cells and mice, respectively.

Results: The nanocomposites specifically targeted tumor cells through enhancing permeability and retention (EPR) effect. Results from in vitro experiments showed that the nanocarriers not only promoted cell apoptosis and reduced the number of cells for chemotherapy, but also promoted accumulation of reactive oxygen species (ROSs). In vivo experiments showed that mice in the nanocomposite-treated group exhibited the smallest tumor sizes and body weights, with no obvious damage to normal tissues and organs.

Conclusion: Taken together, these findings indicated that nanocarriers had an effective inhibitory effect on HCC cells. This safe and multifunctional treatment model was a valuable option for the treatment of HCC, as well as other cancers.

Keywords: Ferroptosis, Hepatocellular carcinoma, Prussian blue, Sorafenib

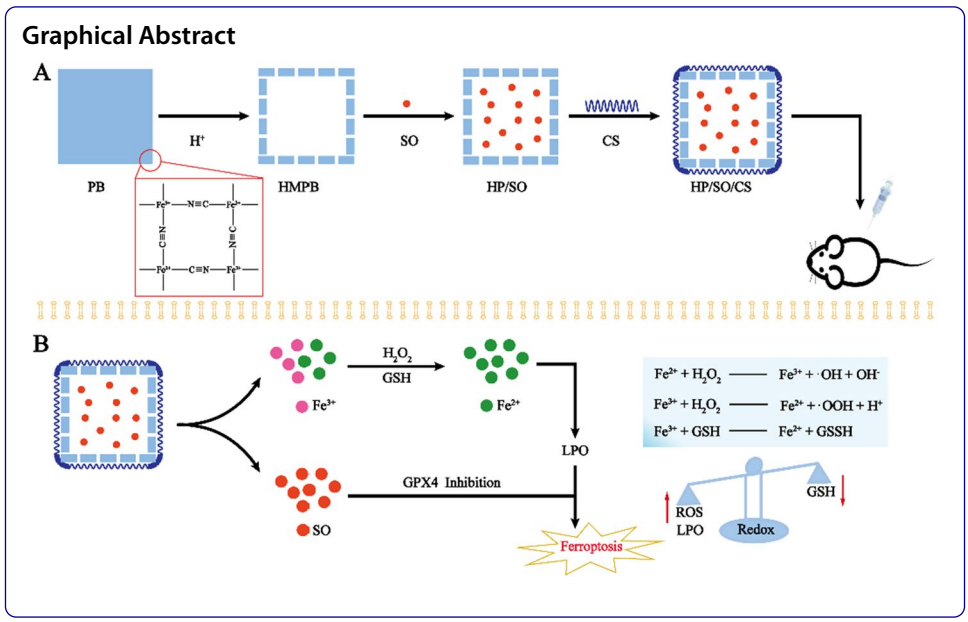

Background

Hepatocellular carcinoma (HCC) is the main cause of cancer-related deaths and a major health concern worldwide (Llovet et al. 2021; Bray et al. 2018). Clinical diagnosis of early-stage patients is difficult, and chemotherapy is the main treatment strategy for patients with advanced HCC (Zhou et al. 2020). At present, sorafenib (SO) as the first-line treatment therapy for HCC, can significantly prolong overall survival times of HCC patients (Wong et al. 2011). Besides, SO is an oral multi-kinase inhibitor that increases the rate of apoptosis, inhibits proliferation and angiogenesis of tumor cells (Palomba et al. 2019). However, long-term single drug therapy is detrimental to the outcome of chemotherapy, mainly including high systemic toxicity, low solubility, low oral bioavailability and chemical resistance (Edis et al. 2021). Therefore, exploring new methods to overcome these shortcomings is imperative to enhance its therapeutic effect.

The recent advancements in the field of nanotechnology have led to more and more applications of nanoparticle-mediated drug delivery for tumor therapy (Jia et al. 2021). Previous studies have shown that nanocarriers can passively target tumors by enhancing permeability and retention (EPR) effect, improving drug targeting, cell uptake, and drug delivery to tumor cells in a continuous, directed, and controlled manner (Dai et al. 2016). Moreover, results from various cancer studies have demonstrated that nanoparticle-mediated drug delivery systems not only have anti-cancer effects, but also exhibit improved bioavailability and minimal side effects compared to free drugs (Wei et al. 2019). Prussian blue (PB) nanoparticles are the first artificial coordination polymer obtained by co-precipitation of an Fe III salt and [Fe II $(CN)_6]^{4-}$ in water. Previous studies have shown that their crystal structure is a face-centered cubic unit cell, where alternating Fe III and Fe II are bridged by the cyano ligands (Laure et al. 2017). These classical nanocarriers, which are composed of Fe^{2+} and Fe^{3+} and have been approved by the FDA, are widely applied in biomedical fields due to their strong magnetism, good biocompatibility and excellent stability among other attributes (Liu et al. 2019). Besides, hollow mesoporous PB

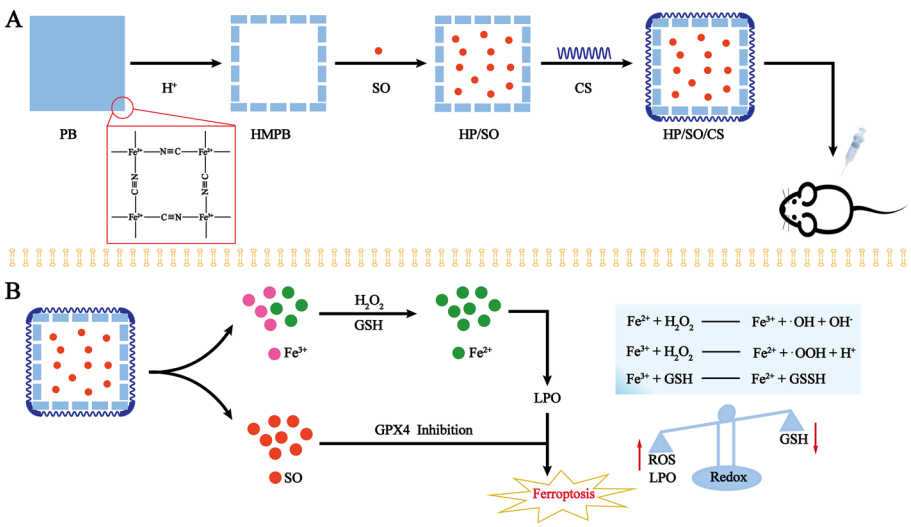

Scheme 1 **A** Synthesis of HP/SO/CS nanocarriers. **B** pH-triggered degradation and drug release of the nanocarriers in the tumor microenvironment (TME), initiating ferroptosis and chemotherapy.

nanoparticles (HMPBs) which are synthesized by controlled chemical etching, with huge cavity gap, are also used as drug carriers for tumor treatment. In addition, the payload in HMPB can be released under mildly acidic conditions, owing to unstable C≡N bond under acid environment (Wu et al. 2020). At the same time, it has the potential to decompose H_2O_2, and convert it into reactive oxygen species (ROS) through Fenton reaction and initiating ferroptosis (Hang et al. 2019).

In this study, we evaluated efficacy of HMPB as nano-delivery carriers for loading SO, with the aim of overcoming drawbacks associated with free SO for effective HCC treatment (Scheme 1). Summarily, SO was encapsulated in HMPB cavity, and coated with acid-unstable chitosan (CS) on its outer layer to form HP/SO/CS nanocomposites. Results showed that CS not only improved pH responsiveness of the nanocarriers, but also enhanced biocompatibility and prevented the drug from prematurely leaking before reaching the tumor site. Results from in vivo assay indicated that the nanocarriers effectively accumulated at the tumor site via the EPR effect. In the tumor microenvironment (TME), the mildly acidic condition caused HP/SO/CS to collapse, thereby releasing Fe^{2+}, Fe^{3+} and SO, initiating ferroptosis and chemotherapy. Interestingly, SO was a promoter of ferroptosis (Liu et al. 2018), which downregulated expression of ferroptosis-related protein GPX4, causing accumulation of lipid peroxide (LPO), promoting ferroptosis and enhancing the therapeutic effect.Scheme 1A Synthesis of HP/SO/CS nanocarriers. B pH-triggered degradation and drug release of the nanocarriers in the tumor microenvironment (TME), initiating ferroptosis and chemotherapy.Scheme 1A Synthesis of HP/SO/CS nanocarriers. B pH-triggered degradation and drug release of the nanocarriers in the tumor microenvironment (TME), initiating ferroptosis and chemotherapy.Scheme 1A Synthesis of HP/SO/CS nanocarriers. B pH-triggered degradation and drug release of the nanocarriers in the tumor microenvironment (TME), initiating ferroptosis and chemotherapy.

Results

Characterization of HP/SO/CS nanocomposites

We used UV–vis absorption spectroscopy to analyze the synthetic structure of HP/SO/CS. Results showed that both PB and HMPB displayed a broad absorption band from 600 to 800 nm, with a strong peak around 720 nm (Fig. 1A) (Cheng et al. 2014). Moreover, a new UV–vis absorption peak appeared in the HP/SO/CS curve at 260 nm, and this was found to belong to the SO peak (Yu et al. 2020). These results affirmed SO encapsulated in HMPB and successful synthesis of HP/SO/CS. Next, we performed a nitrogen adsorption–desorption assay to analyze the specific surface area and porous structure of HMPB, found that HMPB exhibited a typical Langmuir type IV isotherm, indicating the presence of mesopores (Fig. 1B). Its surface area and pore size were 288.0571 m^2/g and 3.94 nm (Feng et al. 2019). Overall, these results suggested that the hollow mesoporous structure could be used as ideal carriers for loading of anti-cancer drugs. The surface zeta potential changed from -23.68 to 28.85 mV in PB and HP/SO/CS, respectively (Fig. 1C), and this was beneficial for cellular uptake in the TME, because the cell membrane is negatively charged. Meanwhile, we used transmission electron microscopy (TEM) to verify successful transformation from PB to HMPB, and finally to HP/SO/CS (Fig. 1D (a-c). Results indicated that HP/SO/CS had well-defined particle about 170 nm (Fig. 1E), which facilitated its entry into cells via the enhanced permeability and retention (EPR) effect. EPR indicated that molecules with sizes that vary from 10 to 200 nm tend to have a higher accumulation rate in the tumor, relative to normal tissues (Kobayashi et al. 2013). Furthermore, results from element map scanning confirmed presence of Fe and F, a characteristic element of HMPB and SO in HP/SO/CS. This demonstrated that HP/SO/CS was successfully synthesized while SO molecules were efficiently loaded into

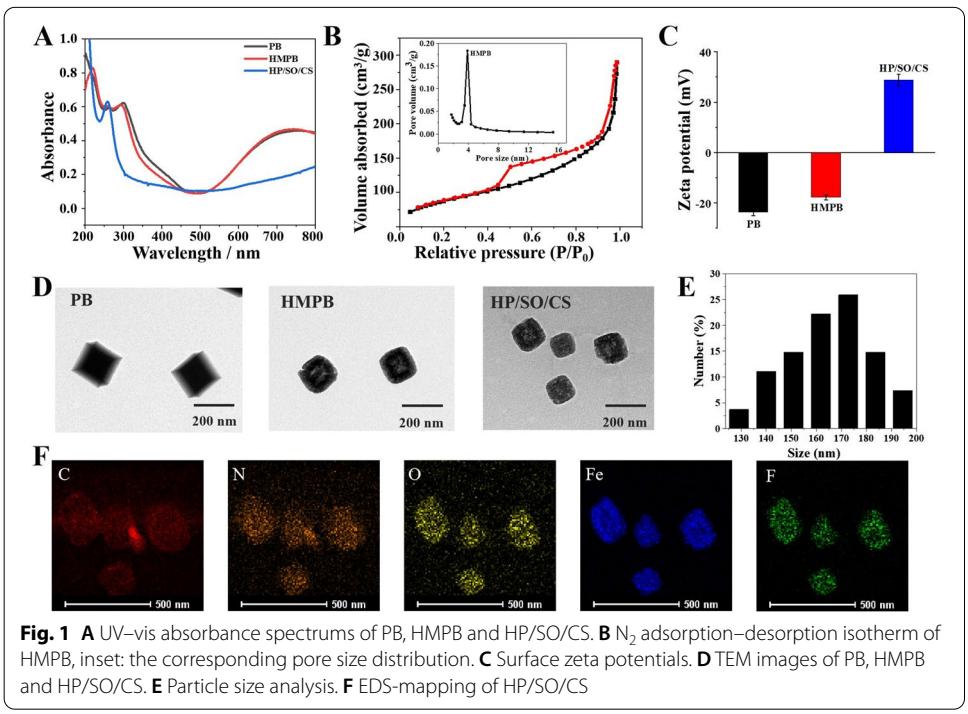

Fig. 1 **A** UV–vis absorbance spectrums of PB, HMPB and HP/SO/CS. **B** N_2 adsorption–desorption isotherm of HMPB, inset: the corresponding pore size distribution. **C** Surface zeta potentials. **D** TEM images of PB, HMPB and HP/SO/CS. **E** Particle size analysis. **F** EDS-mapping of HP/SO/CS

the cavity of HMPB (Fig. 1F). Taken together, these results indicated that the HP/SO/CS nanocomposites were successfully synthesized.

Hemolysis assay

Results from standard hemolysis assay which used to evaluate hemocompatibility of HP/SO/CS nanocomposites, revealed no obvious visible hemolysis effect across all HP/SO/CS-tested samples, relative to visually red positive controls (P). Increasing the concentration to 10 mg/mL resulted in a hemolysis rate of only 0.46%. Results from UV–vis absorption spectroscopy of the supernatant corroborated this finding (Fig. 2B). The negligible hemolytic activity of HP/SO/CS confirmed that the nanoparticles had excellent biocompatibility with blood cells, which was favorable for intravenous administration.

Drug encapsulation and release in vitro

We analyzed efficiency of drug encapsulation and release to ascertain effectiveness of this nanosystem. Briefly, drug encapsulation efficiency was calculated by measuring UV–vis absorbance of the supernatant across varying concentrations of SO and HP/SO/CS nanomaterials according to the SO standard curve (Additional file 1: Fig. S1). Results showed that encapsulation efficiency increased with SO concentration, reaching a maximum at approximately 78% when SO concentration was 500 μg/mL (RSD: 0.26–4.6%) (Fig. 3A). We attributed this high SO encapsulation efficiency to HMPB's distinctive characteristics, including hollow mesoporous structure for drug loading and the effective combination sites (Fe^{2+}, Fe^{3+}) in its structure. This was facile to coordinate with the chemical groups (OH, NH_2).

We also adopted a similar method to calculate efficiency of drug release under different pH environments. Specifically, PBS at pH values of 7.4, 6.5, and 5.5 were used to simulate neutral healthy body fluids and intra-tumoral mildly acidic tumor microenvironment (TME), respectively (Wu et al. 2021). Results showed that less than 25% of SO was released in PBS (pH 7.4), which was due to stability of the nanocomposites, although this drug release ability dramatically increased under a mildly acidic environment (Fig. 3B). A markedly higher proportion of the drug (87%) was released at pH 5.5 than at pH 6.5 (69%). This indicated that minimizing both off-targeted release and side effects of chemotherapeutics before reaching special area which was imperative to improving anti-tumor efficiency. This phenomenon might contribute to the C≡N bonds in HMPB and the NH_2 groups in CS having no stable existence in weak acidic

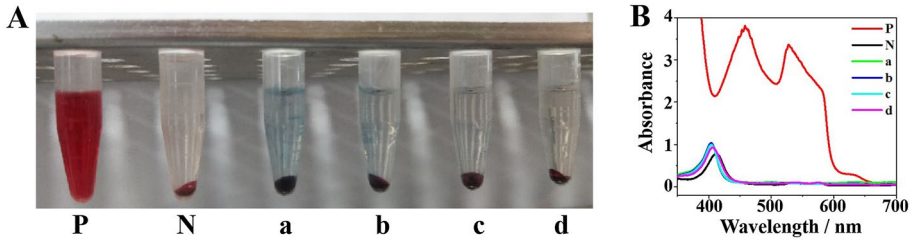

Fig. 2 Hemolysis assay after incubation with different concentrations of HP/SO/CS. **A** Photograph. **B** UV–vis absorbance spectra of supernatant. *P* positive control, *N* negative control, *a* 10 mg/mL, *b* 5 mg/mL, *c* 2.5 mg/mL, *d* 1.25 mg/mL

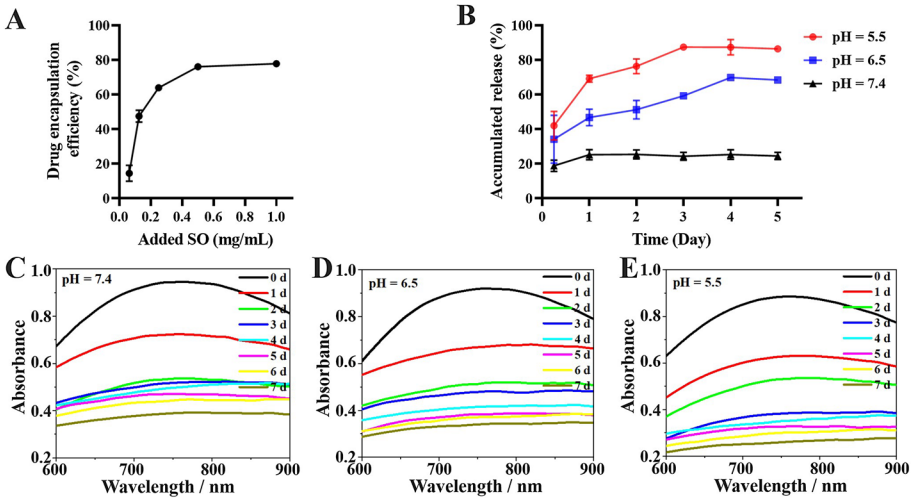

Fig. 3 **A** Drug encapsulation efficiency. **B** Drug release efficiency at different pH values. **C**–**E** UV–vis absorption peaks of HP/SO/CS degradations at different pH values

environment. Additionally, UV–vis results revealed that absorption peaks of HMPB about 600–800 nm in weak acidic environments (pH 6.5 and pH 5.5) were significantly lower, and the absorbance of the environment pH 5.5 was lower than pH 6.5 (RSD: 0.79–13.8%), than those under a neutral environment (pH 7.4) (Fig. 3C–E). Taken together, these results demonstrated that HP/SO/CS were degraded under a mildly acidic environment, and HP/SO/CS could produce a durable therapeutic performance under a weakly acidic TME by combining ferroptosis with chemotherapy.

Wound-healing assay in vitro

We used a cell matrix wound healing assay to evaluate the effect of HP/SO/CS nanocomposites on cell migration abilities. Results revealed similar wound-healing ability in HMPB and PBS treatment groups, whereas a slightly lower cell number and wound healing ability were recorded in the SO treatment group relative to PBS and HMPB groups (Additional file 1: Fig. S2). These results suggested that a combination therapy (chemotherapy and ferroptosis) had better efficacy in killing and reducing the wound healing ability of cells, compared with chemotherapy and nanocarrier treatment alone.

Tumor cell-killing ability in vitro

The present study evaluated tumor cell-killing potential of HP/SO/CS in vitro using cell counting kit-8 (CCK-8) assays coupled with live/dead (AO/EB) staining. We found that neither HMPB nor HP/SO/CS treatment exhibited significant influence on cell viability at pH 7.4 (normal medium). This indicated that there was excellent cytocompatibility between HMPB and HP/SO/CS. Free SO had a similar result with that of HMPB and HP/SO/CS, whereas the cell viabilities gradually decreased with elevated concentration of SO (Fig. 4A(a); RSD: 0.23–4.6%). In addition, the results

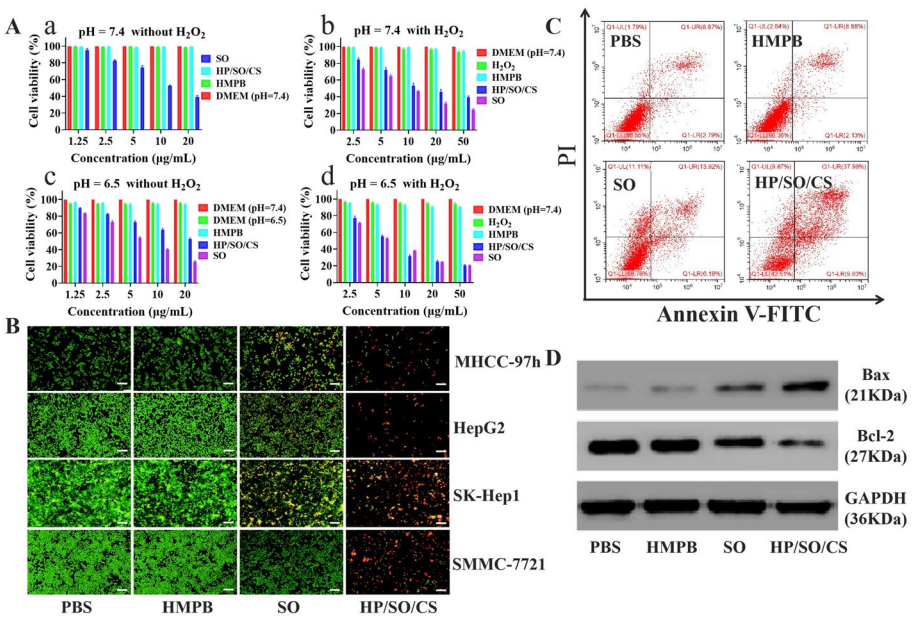

Fig. 4 **A** Cell viability of MHCC-97 h cells treated with different concentrations of HMPB, SO and HP/SO/CS in different pH and H_2O_2 environments. **B** Fluorescence images of live/dead staining in MHCC-97 h, HepG2, SMMC-7721 and SK-Hep1 cells. Live cells (green), dead cells (red). After treatments with PBS, HMPB, SO and HP/SO/CS in MHCC-97 h cells, **C** FCM analysis of using FITC labeled Annexin V and **D** Western blot analysis of Bax and Bcl-2 expression

revealed that only under a relatively high SO concentration that the chemotherapy alone could exert effective cancer cell killing effect.

Acidic tumor microenvironment usually exists in solid tumors due to glycolytic metabolism and incomplete vascularization (Huang and Zong 2017). The present study compared the tumor-killing ability of HP/SO/CS at normal medium (pH 7.4) and acidic medium (pH 6.5). Notably, it was found that the acidic environment (pH 6.5) significantly enhanced the efficacy of HP/SO/CS and SO, which could be attributed to the special internalizing mechanism of nanoparticles (endocytic pathways and lysosomal transport) (Li et al. 2017), resulting in a comparatively high drug concentration in the tumor cells in a short period of time. Second, it was suggested that the weakly acidic environment could break the acid-unstable C≡N bonds in HMPB and the NH_2 groups in CS, releasing chemotherapeutic drug SO, free Fe^{2+}, and Fe^{3+}, hence initiating chemotherapy and ferroptosis treatment. Third, the acidic conditions could have improved solubility of SO and made the SO molecules positively charged, which enhanced ability of the molecules to enter the tumor cells (Fig. 4A (c, d); RSD: 0.43–2.3%).

Further, excessive H_2O_2 in the TME also had a great impact on the effect of HP/SO/CS, because Fe^{2+} in HMPB could have produced Fenton reaction with H_2O_2 (initiating ferroptosis treatment) and thus increasing the content of reactive oxide species (ROSs) and reducing consumption of lipid peroxides (LPO). As described in Fig. 4A(b, d), it was shown that the cell activity of HP/SO/CS was significantly reduced after 50 μM of H_2O_2 was added in the treatment groups. However, it was evident that H_2O_2 alone had no significant effect on cell activity (RSD: 0.46–2.3%).

Calcein acetoxymethyl ester AO/EB staining assay was also carried out to visualize living and dead cells through fluorescence and the results were consistent with those of the CCK8 assay (Fig. 4B). It was found that strong green fluorescence signals were distinctly observed in the control (PBS) and HMPB groups, which revealed the ineffectiveness of the treatments in killing the cancer cells. Further, strong red fluorescence was expressly presented in the group treated with HP/SO/CS and the number of tumor cells was also significantly reduced. However, only a few of red fluorescence and no significant change in the number of cells were found in the SO group. This further proved that chemotherapy alone had insignificant potential to kill the cancer cells, whereas combination of chemotherapy and ferroptosis significantly decreased activity of the MHCC-97 h tumor cells.

The phenomenon of cell death was further supported by the findings of flow cytometry (FCM). During FCM analysis the differently treated MHCC-97 h tumor cells were stained with FITC-labeled Annexin V and PI for assessment of the cell death. The FCM analysis indicated that a combined treatment of HP/SO/CS was able to induce effective tumor cell apoptosis as compared with those of mono-therapies and thus showing synergistically enhanced therapeutic efficacy of the treatments (Fig. 4C).

In addition, Western blotting (WB) assays were also employed to ensure reliability of FCM assay. The level of the two key apoptosis signaling associated proteins (Bax and Bcl-2) were detected in MHCC-97 h cells (Fig. 4D). It was found that the level of Bax which promotes apoptosis was up-regulated, whereas the expression of anti-apoptosis protein Bcl-2 was decreased. The results were consistent with those of the FCM assay.

To verify the effect of HP/SO/CS on cell proliferation, the EdU cell proliferation assay was carried out. The cells in the groups treated with HP/SO/CS showed a higher proliferation inhibitory effect than in the other groups. Meanwhile, the effect of HMPB on cell proliferation was similar as that of the PBS on the tumor cells, but the influence of SO on cell proliferation was negligible (Additional file 1: Fig. S3).

Cell uptake in vitro

To conveniently monitor the uptake efficiency of HP/SO/CS nanocarriers in MHCC-97 h cells, SO was replaced with fluorescence reagent of fluorescein isothiocyanate (FITC) to label nanomaterials because there was no fluorescence that was being observed in SO under CLSM. After incubation of nanocarriers with HP/FITC/CS for different time intervals (0, 4, 8, and 12 h), green fluorescence signal of FITC in tumor cells gradually increased as displayed on the CLSM image (Fig. 5A). In addition, results of FCM as presented in Fig. 5B also confirmed that the fluorescence intensity of FITC gradually increased with time. Moreover, results of the biological transmission electron microscopy (Bio-TEM, Fig. 5C) also showed that there were notable cube structures of the nanocomposites which were visible in cells. Therefore, the described results evidently showed that HP/SO/CS nanocomposites could effectively be internalized into cells.

The ability of ferroptosis treatment of HP/SO/CS nanocarriers in vitro

The present study also recognized cellular ROSs as crucial biomarker of ferroptosis (Lippmann et al. 2020). Therefore, 2′,7′-dichlorofluorescein diacetate (DCFH-DA) was

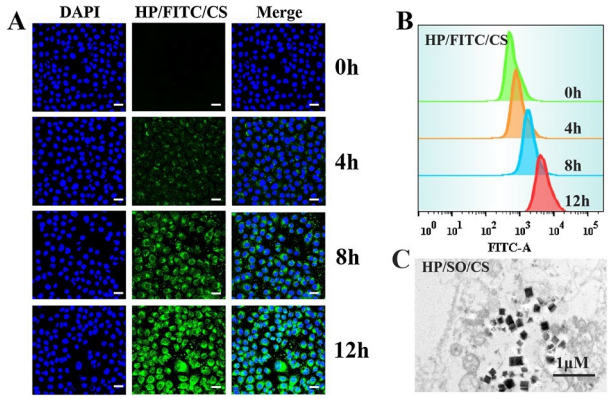

Fig. 5 **A** CLSM images of HP/FITC/CS in MHCC-97 h cells after the indicated time points. **B** FCM assays and **C** Bio-TEM imaging after MHCC-97 h cells were treated with HP/FITC/CS, HP/SO/CS for 12 h, respectively

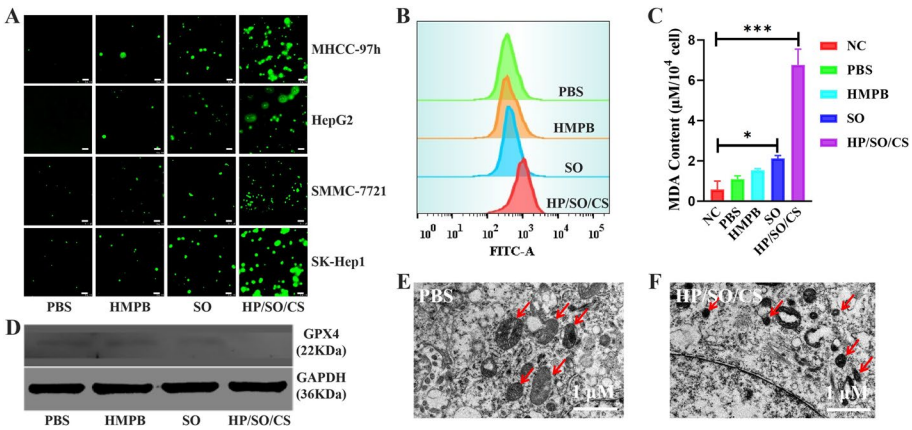

Fig. 6 **A** CLSM images of ROSs production in MHCC-97 h, HepG2, SMMC-7721 and SK-Hep1 cells. **B** FCM assays. **C** MDA content production and **D** WB analysis the expression of GPX4 after MHCC-97 h cells were treated with PBS, HMPB, SO and HP/SO/CS for 24 h. *$p < 0.5$, and ***$p < 0.001$. **E**–**F** Bio-TEM imaging after MHCC-97 h cells were treated with PBS and HP/SO/CS for 24 h

employed as the ^{1}O probe to detect generation of ROSs through CLSM observation and FCM quantification. In the CLSM observation (Fig. 6A), it was noted that there was much stronger fluorescence intensity in MHCC-97 h, HepG2, SMMC-7721 and SK-Hep1 cells after incubation with HP/SO/CS for 24 h. In addition, although CLSM observation showed reduced generation of ROSs in both HMPB and SO groups, it was evident that the overall effect of the therapy was negligible. These implied that the individual impact of SO and Fe-derived HMPB on induction of ferroptosis were nearly null, but a combination therapy could produce significant results. Flow cytometry assessment also showed similar results to those of the CLSM observation (Fig. 6B). Therefore, the reasons for the enhancement of HP/SO/CS in cancer treatment were evidently elucidated.

Besides, lipid peroxide (LPO) inside cells were recognized as a crucial biomarker of ferroptosis. It had been reported that accumulation of LPO contributes to the lethality of ferroptosis (Agmon et al. 2018). In this study, it was found that HMPB decomposed to produce Fe^{2} and Fe^{3+} under mildly acidic conditions, which could promote

the production of LPO through the Fenton reaction. Second, SO could have reduced the consumption of LPO by inhibiting the activity of GPX4 enzyme. These reasons resulted in a large amount of LPO to be accumulated. In addition, malondialdehyde (MDA) which served as an advanced LPO end-product, was expressed in elevated levels throughout the MDA assay process (Aly et al. 2013) (RSD: 0.15–0.77%). Therefore, MDA assay was conducted in MHCC-97 h cells, after treatment with varying treatments (Fig. 6C). Results revealed that there was an elevated MDA content in the HP/SO/CS combined treatment groups as compared with the MDA content in the groups treated with solely HMPB and SO. Apparently, it was found that the PBS group had the least MDA generated.

In addition, we found that SO which is a hydrophobic ferroptosis promoter was encapsulated in the nanoplatform and co-induced cell ferroptosis together with Fe derived from HMPB. The level of GSH was generally regarded as the marker of strength when evaluation of ferroptosis because cytotoxic •OH produced from Fe. Fenton reaction in ferroptosis which would oxidize and diminish the level of the intracellular GSH. As presented in Additional file 1: Fig. S4, the HP/SO/CS-treated cells exhibited a relatively lower level of GSH as compared with the PBS-treated cells. However, the depletion in GSH level of the other two groups treated with only HMPB or SO were almost negligible, whereas a negative correlation between MDA and GSH level was observed.

Besides, SO is used as a promoter of ferroptosis by down-regulating the expression of GPX4 (Bai et al. 2019) which is usually considered as one of the biomarkers of ferroptosis. The WB assay was employed to evaluate the GPX4 expression in MHCC-97 h tumor cells. It was evident that treating cells with HP/SO/CS could significantly downregulate expression of GPX4 as compared to control group (Fig. 6D). However, the individual HMPB or SO treatment groups could not achieve a similar effect but had similar expression effect with that in the PBS group (Fig. 6D).

Further, we used Bio-TEM analysis to distinguish ferroptosis from other forms of cell death. It was found that the cell treated with HP/SO/CS appeared to have significantly smaller mitochondria, increased membrane density, and decreased or disappeared mitochondrial ridge as compared with PBS group (Fig. 6E, F) (Guo et al. 2021). Therefore, the results of our study implied that the HP/SO/CS nanocomposites could destroy mitochondrial membrane and induced typical morphological changes of ferroptosis.

Biodistribution of HP/FITC/CS in vivo

To evaluate tumor targeting ability of HP/SO/CS in vivo, free FITC and HP/FITC/CS were prepared and intravenously injected into tumor-bearing mice for observation at indicated time points. The position of the tumor in the mouse with free FITC-injected group did not exhibit strong fluorescence (Fig. 7). This demonstrated that free FITC lacks strong targeting ability on the tumor. On the contrary, in the group injected with HP/FITC/CS, the accumulation of fluorescence in the tumor site gradually increased with time, and completely disappeared at 24 h. This suggested that the nanocomposites could accumulate efficiently at the tumor site and properly metabolized, which may attribute to excellent effect of EPR and biocompatibility of the nanocarriers.

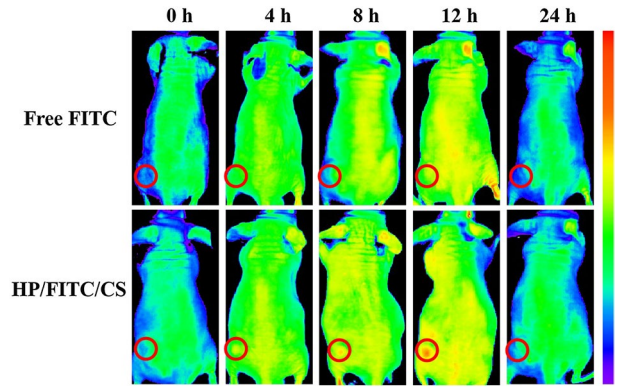

Fig. 7 In vivo imaging of biodistribution of free FITC and HP/FITC/CS at different time points (circles indicate tumor location)

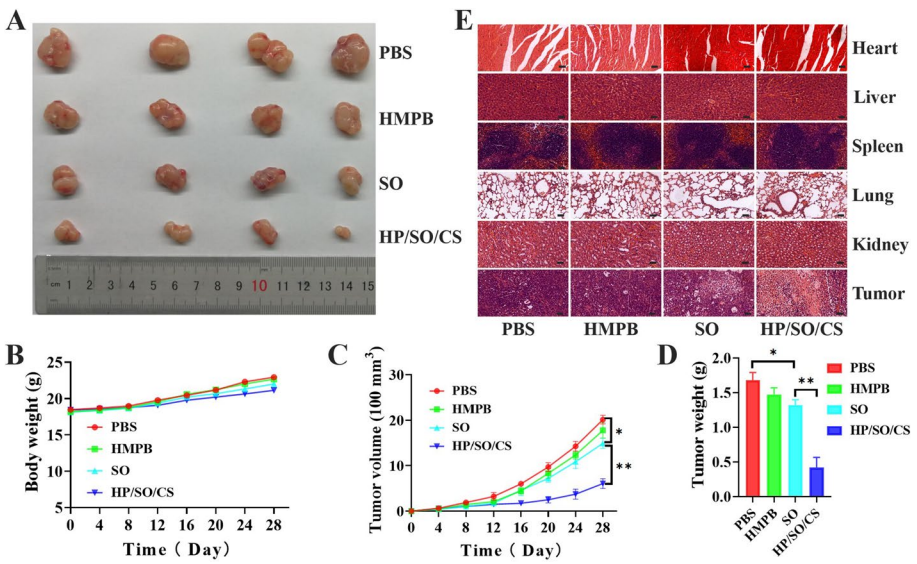

Fig. 8 **A** Photographs of the final tumor size after various treatments. **B** The change of mice body weight during the treatment period. **C** Tumor volume growth curves of mice with indicated treatments. **D** Final tumor weights after various treatments. *p < 0.05, and **p < 0.01. **E** H&E staining of the heart, liver, spleen, lung, kidney and tumor tissues with different treatments

Combination treatment efficacy of HP/SO/CS in vivo

When the tumors reached about 150 mm^3, MHCC-97 h tumor-bearing mice were randomly divided into 4 groups for observation of their body weights, tumor volumes, and tumor weights of mice after different intravenous injection (PBS, HMPB, SO, HP/SO/CS) to investigate the anti-tumor efficacy of combination therapy in vivo. Firstly, the mice were killed for tumor harvest and the effect of treatments was examined using photographs at the end of treatment. It was found that combination therapy showed the best results and tumors in the group were the smallest (Fig. 8A). Moreover, it was noted that the mice in all groups did not reveal any significant weight loss, suggesting that the treatment had no significant cytotoxic effect on other normal tissue in vivo (Fig. 8B). At

the same time, the HP/SO/CS group exhibited the best anti-tumor efficacy, more significant tumor volume reduction, and lower tumor weight as compared with other groups (Fig. 8C, D).

Finally, to further confirm the most potent therapeutic efficacy, hematoxylin and eosin (H&E) staining was performed on the main organs (heart, liver, spleen, lung, and kidney) and tumor tissues, mice with PBS treatment were used for comparison (Fig. 8E). It was found that there were no significant pathological toxicity characteristics in the main organs. These demonstrated the safety of HP/SO/CS in vivo, which may be attributed to excellent biocompatibility of CS and low cytotoxicity of HMPB. Further, it was found that almost all the tumor cells maintained cellular integrity morphology in the PBS, HMPB, and SO treated group. On the contrary, it was noted that large quantities of cells were destroyed in the HP/SO/CS group. The H&E staining of tumor slice showed that the cell-killing effect was rather significant in the HP/SO/CS group. Therefore, these results illustrated that treatment with a combination of chemotherapy and ferroptosis had a significant effect on HCC treatment.

Discussion

SO was the first systematic therapy to be approved for HCC and had been approved by the US FDA for the pharmaceutical treatment of unresectable HCC (Preziosi et al. 2019). However, it had disadvantages of low solubility, low bioavailability, lack of targeting and higher systemic toxicity (Kong et al. 2021). In recent years, nano-drug delivery systems had been widely adopted to overcome these shortcomings (He et al. 2010). The encapsulation of nanoparticles could significantly prolong the blood circulation time of chemotherapy drugs, enhance the EPR effect, facilitate passive targeting of tumor sites, control drug release, and increase bioavailability. Such as Cai et al. (2015) synthesized Mn-containing Prussian blue analogue (HMPB-Mn) using HMPB as nanocarrier. Interestingly, they discovered that HMPB-Mn was highly sensitive to pH-trigger to release Mn^{2+} in the site of interest (e.g., tumor site) which made HMPB-Mn as a smart carrier for tumor diagnosis. Furthermore, the hollow mesoporous structure and high surface area endowed HMPB-Mn with high drug loading capacity for tumor chemotherapy.

In this study, HMPB was used as a nanocarrier to load chemotherapy drug SO, and HP/SO/CS nanocomposite was synthesized for the treatment of hepatocellular carcinoma by virtue of the excellent characteristics of HMPB. The average diameter of HP/SO/CS was 170 nm and zeta potential was 28.85 mV, which contributed to the entry of HP/SO/CS into tumor cells through EPR effect. In vitro experiments showed that HP/SO/CS had good blood compatibility, the hemolysis rate was only 0.46% even at the concentration of 10 mg/mL. And it also had high drug loading and release efficiency, the loading efficiency was 78%, release efficiency was 87% (pH 5.5) and 69% (pH 6.5), respectively. Intracellular experiment results suggested that cells had excellent uptake capacity for the HP/SO/CS nanocarrier, and it could slow down the wound healing ability, had no significant effect on the activity of HCC cells under normal physiological conditions (pH 7.4), but showed a good killing effect on HCC cells in tumor microenvironment (pH 6.5 with 50 μM of H_2O_2). When the HP/SO/CS nanocarriers concentration was 10 μg/mL, the cell activity was 24%. AO/EB, WB and FCM apoptosis test confirmed the similar result. Ferroptosis assay showed that HP/SO/CS nanocomposites could damage tumor

cells by promoting ROS and LPO production and down-regulating the expression of ferroptosis-related protein GPX4. In vivo experiments showed that compared with the control group (PBS, HMPB and SO treatment group), HP/SO/CS treatment group had the smallest tumor volume, the lightest body weight, and had no obvious damage to normal tissues and organs, such as heart, liver, spleen, lung and kidney. These above experimental results proved that HP/SO/CS nanocomposites had good targeting, excellent biocompatibility and better inhibition of tumor growth.

In this experiment, there were some deficiencies worth of our consideration. On the one hand, the water-solubility of Fe-based nanocarriers were not well, so we can consider encapsulating some water-soluble substances on it to increase its solubility in subsequent experiment. On the other hand, only relying on EPR effect of nanocarriers to enhance its targeting may not be as ideal as expected. In following studies, connecting of some tumor-specific targets or magnetic targeting could be considered to enhance its targeting. What's more, photothermal therapy (Huang et al. 2006), starvation therapy (Zhang et al. 2021), gene editing (Wu et al. 2014), etc., were also attracting more and more attention as new therapeutic methods. A combination of several treatments may be considered to achieve better tumor treatment outcomes in the follow-up study.

Conclusion

The present study successfully developed a pH-responsive tumor-targeted nano-drug system (HP/SO/CS) for the treatment of HCC by combining chemotherapy with ferroptosis which share mutually promoted effect. The hemolysis and cytotoxicity assays evidently showed that the system had excellent blood compatibility and ultra-low side effects on cells. Anti-tumor assay in vitro demonstrated that the treatment could promote the accumulation of ROS, LPO and had excellent killing effect on MHCC-97 h cells. Moreover, WB experiments showed that the nanocarriers could upregulate apoptosis-related protein Bax, downregulate anti-apoptosis-related protein Bcl-2, and decrease expression of ferroptosis-related protein GPX4, hence improving the therapeutic effect of HCC. In vivo experiments also showed that the tumor volume of mice treated with HP/SO/CS was the smallest, and there was no significant damage to other body tissues and organs in the mice. Therefore, the results of the present study suggested that HP/SO/CS nanocomposites held great potential as an effective nanotherapeutic, which might provide new approaches ideal for other tumor diagnosis and treatment in clinical practice.

Materials and methods

Materials

$K_3[Fe(CN)_6]0.3H_2O$, hydrochloric acid (HCl, 36.0% ~ 38.0%), chitosan (CS) and polyvinylpyrrolidone (PVP, K30) were purchased from Sigma-Aldrich (St. Louis, MO, USA). Hydrogen peroxide (H_2O_2, 30.0%), glutaraldehyde (25%, GA), sorafenib (SO), fluorescein isothiocyanate (FITC) and dimethylsulfoxide (DMSO) were supplied by Solarbio Inc. (Beijing, China). CCK8 and EdU-488 cell proliferation kits, 2',7'-dichlorofluorescein diacetates (DCFH-DA), 4',6-diamidino-2-phenylindole dihydrochloride (DAPI), glutathione (GSH) and 5,5-dithiobis-2-nitrobenzoic acid (DTNB) were bought from Adamas-beta®, Titan technology co., Ltd. (Shanghai, China). All chemical reagents were analytical

grade, and used directly without further purification. Dulbecco's modified Eagle medium (DMEM), fetal bovine serum (FBS), trypsin–EDTA and phosphate-buffered saline (PBS) were obtained from Gibco-BRL (Burlington, ON, Canada).

Characterization of nanoparticles

Morphology of the nanoparticles were analyzed using a transmission electron microscopy (TEM, JEM 1200EX, JEOL Ltd., Tokyo, Japan), while zeta potential of the nanocomposites were determined by a NanoBrook particle sizer. Ultraviolet–visible (UV–vis) absorption of the nanocarriers were measured using a UV-2450 spectrophotometer (Shimadzu, Tokyo, Japan), whereas particle sizes of HP/SO/CS were analyzed by Nano Measurer 1.2 software. HMPB's specific surface area and corresponding pore-size distribution were determined on a Micromeritics Tristar 3000 system (ASAP, 2460, Micromeritics, USA), using the nitrogen (N_2) adsorption–desorption isothermal method.

Preparation of HMPBs

HMPBs were synthesized according to the protocol described by Cai et al 2015 with slight modifications. Firstly, 132 mg of $K_3[Fe(CN)_6]\cdot 3H_2O$ and 3 g of PVP were dissolved in 0.01 M 40 mL HCl solution, and stirred using a magnetic stirrer until a clear yellow solution was obtained. Next, the mixture was incubated in a water bath, maintained at 80 °C for 24 h. The mixture was centrifuged at 13,000 rpm for 20 min, thoroughly washed several times with deionized water and ethanol, then vacuum-dried to obtain cubic mesoporous Prussian blue nanoparticles (PBs). Next, PBs were transformed into hollow mesoporous Prussian blue (HMPBs) using controlled chemical etching. Briefly, 20 mg PB nanoparticles and 100 mg PVP were dissolved in 20 mL HCl solution (1.0 M), stirred for 3 h at room temperature, then autoclaved at 140 °C for 4 h in a Teflon vessel. The mixtures were cooled to room temperature, centrifuged, rinsed with ethanol and deionized water and finally freeze-dried to obtain HMPBs.

Preparation of HP/SO/CS and HP/FITC/CS nanocomposites

Sorafenib (SO) was loaded onto the HMPB nanoparticles as follows: firstly, HMPB and SO were dissolved in DMSO (at equal concentrations of 1 mg/mL), then equal volumes (5 mL) of SO and HMPB solutions mixed at 37 °C for 24 h with magnetic stirring. Subsequently, the SO-loaded HMPBs (HP/SO) were collected through centrifugation, washed with water and dried under a vacuum. Finally, the obtained sediments were dispersed in 0.01 M NaOH and 0.25 mg/mL CS mixture solution (V/V = 1:1) to form HP/SO/CS nanocomposites. FITC-labeled HP/CS nanocomposites were prepared using a similar procedure to that of HP/SO/CS, except that SO was replaced by fluorescein isothiocyanate (FITC).

SO encapsulation and in vitro release

SO encapsulation

HMPB (1 mg/mL) were incubated with different SO concentrations (0.0625, 0.125, 0.25, 0.5 and 1 mg/mL) in 5 mL PBS solution, stirred at room temperature for 24 h, then SO-loading HMPBs collected by centrifugation. Next, we employed UV–vis absorption spectroscopy (at an absorption intensity of 260 nm) to measure the concentration of

unbounded SO in the supernatant. SO standards were also prepared at concentrations of 1.5625, 3.125, 6.25, 12.5, 25, 50, 100 and 200 μg/mL, their UV–vis absorption peaks were measured and used to draw the standard curve. Efficiency and capacity of SO drug encapsulation were calculated using the following formula:

$$\text{Encapsulation efficiency} = (\text{total}_{\text{SO}} - \text{unbounded}_{\text{SO}})/\text{total}_{\text{SO}} \times 100\%,$$

$$\text{Encapsulation capacity} = (\text{total}_{\text{SO}} - \text{unbounded}_{\text{SO}})/(\text{total}_{\text{HMPB}} + \text{total}_{\text{SO}}) \times 100\%.$$

SO release

HP/SO/CS nanocomposites (1 mg/mL) were dissolved in PBS at different pH values (5.5, 6.5 and 7.4), and incubated in an oscillating chamber maintained at 37 °C. The supernatants were collected and absorptions measured after 0, 1, 2, 3, 4 and 5 d. Finally, efficiency of SO release was calculated as described above.

Assessment of biodegradability of HP/CS

HP/CS (30 mg) was dissolved in PBS (30 mL) at different pH values (7.4, 6.5, 5.5), and incubated at 37 °C in an oscillating chamber. Subsequently, absorption peaks of the solution were measured in the range of 600–900 nm by using UV–vis spectroscopy at different time points (0, 1, 2, 3, 4, 5, 6 and 7 days).

Hemolysis assay

Hemolysis assay was performed as described by Zhao et al. 2017. Briefly, fresh anticoagulant blood was obtained from the First People's Hospital of Chongqing Medical University. Red blood cells (RBCs) were centrifuged at 3000 rpm for 3 min, rinsed several times with sterile isotonic PBS solution until the supernatant was colorless and transparent, then diluted tenfold with PBS. Next, 100 μL diluted RBCs suspension were mixed with 900 μL of HP/SO/CS (at various concentrations of 10, 5, 2.5 and 1.25 mg/mL), vortexed and incubated at 37 °C for 1 h. At the same time, 100 μL of RBC solution dissolved in pure water and PBS were used as positive and negative controls, respectively. The mixtures were centrifuged at 3000 rpm for 3 min, supernatants collected and their absorbance measured at 541 nm on a UV–vis absorption spectrometer. The rate of hemolysis was calculated using the following equation: hemolysis (%) = $(I/I_0) \times 100\%$, where I and I_0 denote absorbance of the experimental and negative control groups, respectively.

Cell culture

HCC cell lines (MHCC-97 h, HepG2, SMMC-7721 and SK-Hep1) were purchased from the Chinese Academy of Sciences Cell Bank, and cultured in Dulbecco's modified Eagle medium (DMEM) medium (Gibco, Grand Island, NY, USA) supplemented with 10% fetal bovine serum (FBS, Gibco) and 1% penicillin–streptomycin. The cultures were incubated in a humidified incubator, maintained at 5% CO_2, and 37 °C.

Cytotoxicity assays

Cytotoxicity assays were performed as previously reported by Hu et al. (2019). Briefly, MHCC-97 h cells were seeded into 96-well plates, at a density of 5×10^3 cells per well,

and cultured in standard cell media for 24 h. Then culture medium was changed and cells incubated with complete medium supplemented with different concentrations of HMPB, SO and HP/SO/CS. Notably, HMPB and HP/SO/CS had a similar concentration of HMPB (2.5, 5, 10, 20 and 50 μg/mL). The contents were incubated again for 24 h. Then 10 μL Cell Counting Kit8 (CCK8) solution added to each well followed by 2 h incubation. Finally, the optical density (OD) of each well was measured at 450 nm using a microplate reader (Bio-Rad, Model 550, USA), and relative cell viability was calculated using the following equation: cell viability (%) = $(OD_{sample}/OD_{control}) \times 100\%$. Where OD_{sample} represents the absorbance of the sample, $OD_{control}$ represents the absorbance of the control group.

Cell viability assays

To analyze cell survival and death, MHCC-97 h, HepG2, SMMC-7721 and SK-Hep1 cells were seeded into 6-well plates, allowed to reach a confluence of about 70%, then the original culture media replaced with fresh one containing HMPB (10 μg/mL), SO (5 μg/mL), and HP/SO/CS (HMPB 10 μg/mL + SO 5 μg/mL). Samples treated with PBS were used as controls. The cultures were incubated for 24 h, subjected to acridine orange/ethidium bromide (AO/EB) fluorescent staining for 5 min, and observed under a fluorescence microscope (Leica, Germany). Green and red fluorescence indicated live and dead cells, respectively.

Cell proliferation assay

Cell proliferating capacity was analyzed using the Ed Utes. Briefly, MHCC-97 h cells were seeded in 12-well with glass slides until reached a 70% confluence. Next, the original culture medium was replaced with fresh ones containing PBS, HMPB (10 μg/mL), SO (5 μg/mL), and HP/SO/CS (HMPB 10 μg/mL + SO 5 μg/mL), incubated for 24 h. Finally, according to the kit instructions, their fluorescence intensity determined using a confocal laser scanning microscopy (CLSM).

Determination of cell apoptosis

To analyze cell apoptosis, MHCC-97 h cells were seeded 6-well plates and cultured to attain cell confluence about 70%. The medium was replaced with fresh ones containing HMPB, SO, and HP/SO/CS, where the groups of free SO and HP/SO/CS having the same concentration of SO ($C_{[SO]} = 5$ μg/mL), the groups of HP and HP/SO/CS having an equivalent HMPB dosage ($C_{[HMPB]} = 10$ μg/mL). Cells treated with PBS were also included as controls. Treated cells were harvested using trypsin, washed twice with PBS and stained with the Annexin V/PI cell assay kit according to the manufacturer's instructions. Finally, the samples were subjected to flow cytometry (FCM) analysis to measure the rate of apoptosis.

Wound-healing assay

To test the anti-migratory potential of HP/SO/CS, MHCC-97 h cells were seeded into 6-well plates and incubated for 24 h. Next, a pipette tip was used to create a perpendicular scratch in every well, and the debris removed by extensively washing the plate with

PBS. Then cells were incubated with fresh DMEM medium containing HMPB, HP/SO/CS (with an equal HMPB dose of 10 μg/mL), SO (5 μg/mL) for 24 h, not treated as controls. Wound width was then monitored by inverted fluorescence microscope.

Cellular uptake

To monitor intracellular distribution of nanoparticles, MHCC-97 h cells were seeded into 12-well plates, enclosed with glass coverslips and incubated for 24 h. The medium was aspirated out and replaced with fresh one containing 10 μg/mL HP/FITC/CS, followed by incubation for 0, 4, 8, and 12 h. The cells were washed with PBS, fixed in 4% paraformaldehyde, then stained with DAPI for 5 min. The contents were subjected to CLSM, with green and blue fluorescence representing internalized nanoparticles and nuclei, respectively. At the same time, the cells were quantitatively analyzed by FCM to determine the proportions that had taken up nanoparticles. Briefly, cells were digested with trypsin, centrifuged, washed and resuspended in PBS, then subjected to FCM for detection of FITC fluorescence intensity. Next, proportions of cells that had taken up HP/SO/CS were determined via biological transmission electron microscopy (Bio-TEM). Summarily, cells were digested, centrifuged, washed, and resuspended in glutaraldehyde. Next, they were fixed overnight, then sent to Beijing Zhongkebaice Technology Co., LTD for Bio-TEM examination.

Determination of intracellular ROS production

Intracellular ROS production was detected by CLSM and FCM, using dichlorofluorescein diacetate (DCFH-DA, 10 μM) as the probe. Briefly, MHCC-97 h, HepG2, SK-Hep1 and SMMC-7721 cells were seeded in 12-well plates, enclosed with cell slides, and allowed to grow to a 70% confluence. The culture medium was aspirated out and replaced with fresh ones containing HMPB, SO, and HP/SO/CS, followed by a 24 h incubation. Cells in HMPB and HP/SO/CS groups were exposed to the same concentration of HMPB (10 μg/mL), in SO and HP/SO/CS groups were exposed to the same of SO (5 μg/mL) concentrations, and PBS-treated cells in growth media were used as the control. The cells were washed gently with serum-free medium, stained with DCFH-DA, and incubated at 37 °C for 20 min. Finally, glass coverslips containing cells were imaged under CLSM. Besides, ROS content in cell samples was quantitatively measured as a complement to the above results. Briefly, treated cells were collected by digestion, as previously stated then subjected to FCM for analysis of DCFH-DA fluorescence intensity.

Western blot assay

The effects of the nanocarriers on expression of ferroptosis-related protein GPX4 and apoptosis-related protein Bax and Bcl-2 were evaluated by using Western blot assay. Briefly, MHCC-97 h cells were seeded into 6-well plates, allowed to grow to a 70% confluence, and the original culture medium was replaced with fresh ones containing PBS (control), HP, SO, and HP/SO/CS. The concentration of HP and SO substrates in all sample groups were maintained at 10 and 5 μg/mL. The samples were further incubated for 24 h, washed with PBS, and collected via centrifugation. Total proteins were extracted from the cell pellets using the RIPA lysis buffer and quantified using the BCA

protein assay Kit. Equal concentrations of the proteins were separated on 10% SDS–polyacrylamide gel electrophoresis (SDS-PAGE), and transferred to a polyvinylidene fluoride (PVDF) membranes. The membranes were blocked with 5% skim milk, then incubated with primary antibodies against GPX4, Bax and Bcl-2, followed by secondary horseradish peroxidase-conjugated antibodies. Finally, the membranes were imaged with chemiluminescence.

GSH assay

MHCC-97 h cells were treated as previously mentioned (PBS, HP, SO, and HP/SO/CS), collected and washed three times with PBS. Subsequently, the cells were lysed and 100 μL of the lysis was co-incubated with DTNB (40 μM) for 30 min. Cellular GSH was estimated under UV–vis spectroscopy at 410 nm, and the actual GSH content calculated according to the GSH standard curve.

MDA assay

Tumor cells were treated as previously described, namely PBS, HP (10 μg/mL), SO (5 μg/mL) and HP/SO/CS (10 μg/mL), then malondialdehyde (MDA) content was measured using the Thiobarbituric Acid Reactive Substances (TBARS) assay kit.

Establishment of a tumor mouse model

Male nude BALB/c mice (4–6 weeks old) were obtained from the Chinese Academy of Science. The tumor model was established by subcutaneously injecting 150 μL of MHCC-97 h cells (at a density of 1×10^7) into the thigh region of the nude mice. All animal experiments were conducted in accordance with the guidelines of the Animal Management Rules of the Ministry of Health of the People's Republic of China, and the Care and Use of Laboratory Animals of China Pharmaceutical University. All experimental protocols were approved by the Chongqing Medical University and were conducted in strict compliance with protocol procedures.

In vivo assays

After a week of model establishment, mice were intravenously injected with 150 μL of free FITC and HP/FITC/CS, with an equal concentration of FITC (5 mg/Kg). The animals were subjected to target analysis of nanoparticles via imaging of FITC at various time points (0, 4, 8, 12 and 24 h) post-injection using IndiGo Living Imaging 4.4 software system.

Evaluation of anti-tumor efficiency in vivo

When tumors had reached a size of about 150 mm^3, the nude mice were randomly divided into four groups (n = 4), and treated with PBS (control), HMPB (10 mg/ kg), SO (5 mg/Kg) and HP/SO/CS (HMPB 10 mg/Kg + SO 5 mg/Kg) through the tail vein. Treatment was performed thrice (once every seven days) with body weights and tumor volumes measured and recorded after every 4 days. Corresponding tumor volumes were calculated by using the following formula: volume = (length × $width^2$)/2. At the end of the treatment period, the mice were killed, their tumors as well as main organs, namely the heart, liver, lung, spleen, and kidney, were harvested. These tissues

were fixed in 4% paraformaldehyde for two days at 4 °C, embedded in paraffin, cut into small sections. Then stained with hematoxylin and eosin (H&E). Finally, the sections were observed under an optical microscope.

Statistical analysis

All experiments were randomized and conducted in triplicate. All data were expressed as means ± standard deviations (SD) of the mean, with differences between groups determined using paired two-sided Student's t-test. Data followed by $P < 0.05$ were considered statistically significant, while $^{**}P < 0.01$ or $^{***}P < 0.001$ were considered highly significant.

Abbreviations

HCC: Hepatocellular carcinoma; SO: Sorafenib; PB: Prussian blue; PBs: Prussian blue nanoparticles; HMPB: Hollow Prussian blue nanoparticles; EPR: Enhancing permeability and retention; ROSs: Reactive oxygen species; TME: Tumor microenvironment; CS: Chitosan; PVP: Polyvinylpyrrolidone; TEM: Transmission electron microscopy; AO/EB: Acridine orange/ethidium bromide; CLSM: Confocal laser scanning microscopy; DCFH-DA: Dichlorofluorescin diacetate.

Supplementary Information

The online version contains supplementary material available at https://doi.org/10.1186/s12645-022-00111-4.

Additional file 1: Fig. S1. (A) UV-vis absorption peaks of SO in different concentrations. a-h represented 1.5625, 3.125, 6.25, 12.5, 25, 50, 100 and 200 μg/mL of SO. (B) Drawing of SO standard curve. **Fig. S2**. Wound healing assay of MHCC-97h cells after treatments with PBS, HMPB, SO and HP/SO/CS, respectively. **Fig. S3**. CLSM images of EdU cell proliferation staining in MHCC-97h and HepG2 cells after treatments with PBS, HMPB, SO and HP/SO/CS, respectively. Cell nucleus (blue), HP/SO/CS nanocomposites (green). **Fig. S4**. (A) Drawing of GSH standard curve. (B) GSH concentration of MHCC-97h cells after treatments with PBS, HMPB, SO and HP/SO/CS, respectively.

Acknowledgements

We would like to express our gratitude to all those who financed the subject.

Authors' contributions

YH and GLX performed the in vitro assays. TZR and GLX did the in vivo studies. GLX, LYY and YH analyzed the data and wrote manuscript. GLX, LSC and TH designed this study. LSC and TH reviewed the manuscript. All authors read and approved the final manuscript.

Funding

This study was supported by the Basic research and frontier exploration project of Yuzhong District of Chongqing (20180109), the Key Laboratory of Infectious Diseases, CQMU (202004).

Availability of data and materials

Not applicable.

Declarations

Ethics approval and consent to participate

Animal studies were approved by the Ethics Committee of Animal Experiments of Chongqing Medical University.

Consent for publication

Not applicable.

Competing interests

The authors declare that they have no competing interests.

Author details

[1]Key Laboratory of Molecular Biology for Infectious Diseases (Ministry of Education), Institute for Viral Hepatitis, Department of Infectious Diseases, The Second Affiliated Hospital, Chongqing Medical University, 1 Yi Xue Yuan Road, Chongqing 400016, China. [2]Department of Clinical Laboratory, Chengdu Fifth People's Hospital, Chengdu 611130, China. [3]Department of Endocrine and Breast Surgery, The First Affiliated Hospital of Chongqing Medical University, Chongqing, China. [4]Department of Clinical Laboratory, the Sixth People's Hospital of Chengdu, Chengdu, Sichuan, China. [5]Department of Laboratory Medicine, The First People's Hospital of Zunyi City (The Third Affiliated Hospital of Zunyi Medical University), Zunyi 563000, Guizhou, China.

Received: 15 August 2021 Accepted: 11 January 2022
Published online: 29 January 2022

References

Agmon E, Solon J, Bassereau P, Stockwell BR (2018) Modeling the effects of lipid peroxidation during ferroptosis on membrane properties. Sci Rep 8:5155
Aly H, Azhar AS (2013) Methoxychlor induced biochemical alterations and disruption of spermatogenesis in adult rats. Reprod Toxicol 40:8–15
Bai T, Lei P, Zhou H, Liang R, Zhu R, Wang W et al (2019) Sigma-1 receptor protects against ferroptosis in hepatocellular carcinoma cells. J Cell Mol Med 23:7349–7359
Bray F, Ferlay J, Soerjomataram I, Siegel RL, Torre LA, Jemal A (2018) Global cancer statistics 2018: GLOBOCAN estimates of incidence and mortality worldwide for 36 cancers in 185 countries. CA Cancer J Clin 68:394–424
Cai X, Gao W, Ma M, Wu M, Zhang L, Zheng Y et al (2015) A prussian blue-based core-shell hollow-structured mesoporous nanoparticle as a smart theranostic agent with ultrahigh pH-responsive longitudinal relaxivity. Adv Mater 27:6382–6389
Catala L, Mallah T et al (2017) Nanoparticles of prussian blue analogs and related coordination polymers: from information storage to biomedical applications. Coord Chem Rev 346:32–61
Cheng L, Gong H, Zhu W, Liu J, Wang X, Liu G et al (2014) PEGylated prussian blue nanocubes as a theranostic agent for simultaneous cancer imaging and photothermal therapy. Biomaterials 35:9844–9852
Dai Z, Tu Y, Zhu L (2016) Multifunctional micellar nanocarriers for tumor-targeted delivery of hydrophobic drugs. J Biomed Nanotechnol 12:1199–1210
Edis Z, Wang J, Waqas MK, Ijaz M, Ijaz M (2021) Nanocarriers-mediated drug delivery systems for anticancer agents: an overview and perspectives. Int J Nanomedicine 16:1313–1330
Feng T, Wan J, Li P, Ran H, Chen H, Wang Z et al (2019) A novel NIR-controlled NO release of sodium nitroprusside-doped prussian blue nanoparticle for synergistic tumor treatment. Biomaterials 214:119213
Guo Y, Du J, Xiao C, Xiang P, Li X (2021) Inhibition of ferroptosis-like cell death attenuates neuropathic pain reactions induced by peripheral nerve injury in rats. Eur J Pain 25(6):1227–1240
Hang L, Li H, Zhang T, Men D, Zhang C, Gao P et al (2019) Au@Prussian blue hybrid nano-material synergy with chemotherapeutic drug for tumor diagnosis and chemo-dynamic therapy. ACS Appl Mater Interfaces 11:39493–39502
He CX, He ZG, Gao JQ (2010) Microemulsions as drug delivery systems to improve the solubility and the bioavailability of poorly water-soluble drugs. Expert Opin Drug Deliv 7:445–460
Hu JJ, Chen Y, Li ZH, Peng SY, Zhang XZ (2019) Augment of oxidative damage with enhanced photodynamic process and MTH1 inhibition for tumor therapy. Nano Lett 19:5568–5576
Huang R, Zong X (2017) Aberrant cancer metabolism in epithelial–mesenchymal transition and cancer metastasis: mechanisms in cancer progression. Crit Rev Oncol Hematol 115:13–22
Huang X, El-Sayed IH, Wei Q, El-Sayed MA (2006) Cancer cell imaging and photothermal therapy in the near-infrared region by using gold nanorods. J Am Chem Soc 128:2115–2120
Jia R, Teng L, Gao L, Su T, Fu L, Qiu Z et al (2021) Advances in multiple stimuli-responsive drug-delivery systems for cancer therapy. J Nanomedicine 16:1525–1551
Kobayashi H, Watanabe R, Choyke PL (2013) Improving conventional enhanced permeability and retention (EPR) effects; What is the appropriate target? Theranostics 4:81–89
Kong FH, Ye QF, Miao XY, Liu X, Zhang ZJ (2021) Current status of sorafenib nanoparticle delivery systems in the treatment of hepatocellular carcinoma. Theranostics 11:5464–5490
Li R, Xie Y (2017) Nanodrug delivery systems for targeting the endogenous tumor microenvironment and simultaneously overcoming multidrug resistance properties. J Control Release 251:49–67
Lippmann J, Petri K, Fulda S, Liese J (2020) Redox modulation and induction of ferroptosis as a new therapeutic strategy in hepatocellular carcinoma. Transl Oncol 13:100785
Liu T, Liu W, Zhang M, Yu W, Gao F, Li C et al (2018) Ferrous-supply-regeneration nanoengineering for cancer cell specific ferroptosis in combination with imaging-guided photodynamic therapy. ACS Nano 12:12181–12192
Liu B, Wang W, Fan J, Long Y, Xiao F, Daniyal M et al (2019) RBC membrane camouflaged prussian blue nanoparticles for gamabutolin loading and combined chemo/photothermal therapy of breast cancer. Biomaterials 217:119301
Llovet JM, Kulik L, Haber PK, Greten TF, Meyer T, Lencioni R (2021) Locoregional therapies in the era of molecular and immune treatments for hepatocellular carcinoma. Nat Rev Gastroenterol Hepatol 18:293–313
Palomba F, Genovese D, Rampazzo E, Zaccheroni N, Prodi L, Morbidelli L (2019) PluS nanoparticles loaded with sorafenib: synthetic approach and their effects on endothelial cells. ACS Omega 4:13962–13971
Preziosi ME, Zahm AM, Kaestner KH, Wangensteen KJ (2019) LXR agonism and sorafenib treatment as novel combination therapy for hepatocellular carcinoma. Faseb J 33:126–129
Wei Z, Liang P, Xie J, Song C, Tang C, Wang Y et al (2019) Carrier-free nano-integrated strategy for synergetic cancer antiangiogenic therapy and phototherapy. Chem Sci 10:2778–2784
Wong H, Tang YF, Yao TJ, Chiu J, Leung R, Chan P et al (2011) The outcomes and safety of single-agent sorafenib in the treatment of elderly patients with advanced hepatocellular carcinoma (HCC). Oncologist 16:1721–1728
Wu Y, Zhou H, Fa NX, Ying Z, Man Z, Wang Y (2014) Correction of a genetic disease by CRISPR-Cas9-mediated gene editing in mouse spermatogonial stem cells. Cell Res 25:67–79
Wu W, Yu L, Pu Y, Yao H, Chen Y, Shi J (2020) Copper-enriched prussian blue nanomedicine for in situ disulfiram toxification and photothermal antitumor amplification. Adv Mater 32:e2000542
Wu W, Pu Y, Shi J (2021) Dual size/charge-switchable nanocatalytic medicine for deep tumor therapy. Adv Sci (weinh) 8:2002816

Yu XN, Deng Y, Zhang GC, Liu J, Liu TT, Dong L et al (2020) Sorafenib-conjugated zinc phthalocyanine-based nanocapsule for trimodal therapy in an orthotopic hepatocellular carcinoma xenograft mouse model. ACS Appl Mater Interfaces 12:17193–17206
Zhang H, Lu F, Pan W, Ge Y, Cui B, Gong S et al (2021) A dual-catalytic nanoreactor for synergistic chemodynamic-starvation therapy toward tumor metastasis suppression. Biomater Sci 9(10):3814–3820
Zhao R, Li T, Zheng G, Jiang K, Fan L, Shao J (2017) Simultaneous inhibition of growth and metastasis of hepatocellular carcinoma by co-delivery of ursolic acid and sorafenib using lactobionic acid modified and pH-sensitive chitosan-conjugated mesoporous silica nanocomplex. Biomaterials 143:1–16
Zhou T, Liang X, Wang P, Hu Y, Qi Y, Jin Y et al (2020) A hepatocellular carcinoma targeting nanostrategy with hypoxia-ameliorating and photothermal abilities that inhibits metastasis and recurrence combined with immunotherapy. ACS Nano 14:12679–12696

Publisher's Note